

Megahertz Multiple-Receiver Wireless Power Transfer Systems With Power Flow Management and Maximum Efficiency Point Tracking

Minfan Fu, *Member, IEEE*, He Yin, *Student Member, IEEE*, Chengbin Ma, *Member, IEEE*

Abstract—This paper presents systematic analysis and design of a megahertz multiple-receiver wireless power transfer (WPT) system driven by a Class E power amplifier. Both circuit-level and system-level analysis are conducted to discuss the characteristics of the WPT system. In order to simultaneously manage the power flow and maximize the overall system efficiency, a new control scheme is proposed that combines maximum efficiency point tracking (MEPT) and time-division multiplexing (TDM). Through the proposed scheme, receivers with different loading and coupling conditions can be charged by the same transmitter with simplified design and control strategy. Finally, the proposed control scheme is validated using an example 6.78 MHz three-receiver WPT system. The experimental results show that various power requirements can be quickly and stably satisfied, and the overall average system efficiency can reach as high as 71.7%.

Index Terms—Wireless power transfer, multiple receivers, analysis and design, time-division multiplexing, maximum efficiency point tracking

I. INTRODUCTION

Wireless power transfer (WPT) through inductive coupling became increasingly popular during the past years [1]. Besides the non-contacting power delivery, another unique advantage of WPT is the possibility to charge multiple receivers (RXs) such as wearable devices, cellphones, and household appliances, namely multiple-RX WPT systems. There are fundamental works focusing on the analysis of multiple coupling coils under basic compensations [2]–[4]. Meanwhile, various coil configurations and circuits have been developed to improve the transfer characteristics, such as multiple transmitters (TXs) [5], impedance matching networks [6]–[8], and relay coils [9], [10]. Using dual-band or multiple-band concept, it is possible to charge multiple devices with different resonant frequencies [11]–[13]. Several recently published papers discuss the three-dimensional charging by using orthogonal coils

or cavities [14]–[16]. A new technology called MultiSpot can even charge the devices which are worn or carried by the users [17]. All the above works help to speed up the transition from laboratory systems to real multiple-RX applications. However, there are still many unsolved challenges for a practical multiple-RX systems, particularly the system controllability and stability under variations in load and coupling. It is important to specifically develop a suitable configuration and control scheme for multiple-RX systems.

In the conventional design, usually all the receivers are powered at the same time. The control methods implemented at the TX side (frequency tracking, load-independent source, and automatic impedance matching, etc.) can hardly be used to manage the power flow among receivers because they only affect the overall performance [18]–[20]. In a multiple-RX WPT system, uncertainties caused by the loading and coupling variations may dramatically increase due to the varied number of RXs. The interactive relationships among receivers, such as the cross coupling, also further affect the coil efficiency and make the power distribution unpredictable [4]. New design and control schemes are required to achieve power flow management and maintain high overall system efficiency at the same time in multiple-RX systems.

In order to simplify the system design and control, a well-known communication technology, time-division multiplexing (TDM), has been introduced in WPT applications [21]. The TDM-based WPT system does not require all the receivers to be simultaneously powered. This significantly reduces the system uncertainties and totally avoids the adverse effects of the cross coupling [4]. TDM can be directly combined with the existing control approaches originally developed for the one-RX systems. In high-power applications, an early example is the combination of frequency tuning and TDM to maintain system stability [22]. TDM-based WPT systems have also been developed to charge low-power devices. A real TDM-based WPT system is briefly explained in [23] without details in analysis and implementation. Through having different resonant frequencies, one designated device among multiple devices can be selectively and exclusively charged [24]. Meanwhile, the discussion mainly focuses on the coupling coils in the multiple-RX system. A TDM-based transmitter was built to charge arbitrarily distributed devices in a medical application with a power level of several mW and an average efficiency of 5.8% at the worst case of 90° coil misalignment [25]. A TDM-based power control is applied in a three-orthogonal-coil transmitter [16]. The purpose is to focus the power flow

© 2017 IEEE. Personal use of this material is permitted. Permission from IEEE must be obtained for all other uses, including reprinting/republishing this material for advertising or promotional purposes, collecting new collected works for resale or redistribution to servers or lists, or reuse of any copyrighted component of this work in other works.

Manuscript received September 27, 2016; revised December 23, 2016; accepted March 6, 2017 (*Corresponding author: Chengbin Ma*). This work was supported by the Shanghai Natural Science Foundation under Grant 16ZR1416300.

M. Fu is with the Center for Power Electronics Systems, Virginia Polytechnic Institute and State University, Blacksburg, VA 24061, USA (e-mail: minfanfu@vt.edu).

H. Yin and C. Ma are with the University of Michigan-Shanghai Jiao Tong University Joint Institute, Shanghai Jiao Tong University, Shanghai 200240, China (e-mail: yyy@sju.edu.cn; chbma@sju.edu.cn).

directionally towards the targeted areas. The improvement of efficiency is not fully discussed.

This paper proposes a systematic design methodology and develops a new control scheme by combining maximum efficiency point tracking (MEPT) with TDM, which is shown to be particularly suitable for low-power megahertz (MHz) multiple-RX WPT systems. The use of high operating frequency at MHz is attractive for having improved spatial freedom. However, the high operating frequency is challenging when using the conventional hard-switch inverters due to the high switching losses. Therefore, in this paper a Class E power amplifier (PA) is specifically used, which is able to achieve high peak efficiency (theoretically 100%) at MHz [26]. To fully utilize this advantage, the well-known technology, MEPT, is applied to achieve high system efficiency through improving the loading condition of the Class E PA [27]. In addition, via TDM the charging time becomes a new degree of control freedom. Through the on-off control, the transmitter can always work at its preferred power level when charging various receivers with quite different power requirements. This new possibility further improves the overall system efficiency. The TDM-based control also helps to reduce the system complexity and thus improve the stability. To the best of authors' knowledge this paper is among one of the first works to achieve power and efficiency control (from dc to dc) in a multiple-RX MHz WPT system. In order to power different RXs with the same TX, a systematic design methodology is developed to optimize the PA circuit and compensation capacitors of RXs. The input reactance of the rectifier, which is usually ignored, is particularly considered in the circuit parameters optimization. The proposed design methodology enables optimized system efficiency and power transfer capability when charging different RXs. This unique advantage is useful to enhance the functionality and adaptivity of the multiple-RX WPT systems.

II. CIRCUIT-LEVEL ANALYSIS

A. System Configuration

The proposed multiple-RX system consists of one transmitter and n receivers. As shown in Fig. 1, the transmitter includes a Class E PA and a TX coil. Each receiver includes a RX coil, a rectifier, a buck converter, an energy buffer (optional), and a final load. At any time, the TDM-based control can only enable the charging of at most one RX. Generally, the TX is expected to be able to efficiently charge various RXs that may have quite different power requirements. This objective can be partly achieved by optimizing the parameters of PA and compensations of the RXs based on the impedance characteristics of the rectifiers. The below circuit analysis provides the basis for discussing the following design and control aspects.

B. Transmitter

As shown in Fig. 2, the transmitter consists of a classical Class E PA and a TX coil. In the circuit of the PA, there is a transistor S_{TX} , a shunt capacitor C_S , a radio frequency (RF) choke L_F , and a series tuned resonance tank L_0C_0 . L_t , C_t ,

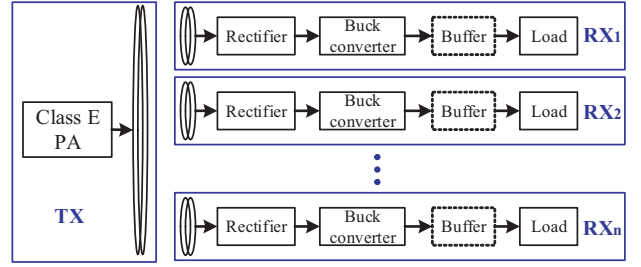


Fig. 1. System configuration.

R_t are the inductance, compensated capacitance, and parasitic resistance of the TX coil. Z_R is the reflected impedance of the receivers. The input impedance of the TX coil, Z_{TX} , is the load of the PA. Given the operating frequency ω , the resonance of TX coil is achieved by letting $\omega L_t = 1/(\omega C_t)$. P_{PA} , P_{TX} and P_{ZR} are the PA input power, PA output power, and transferred power. η_{PA} and η_T are the efficiencies of the PA and TX coil, respectively.

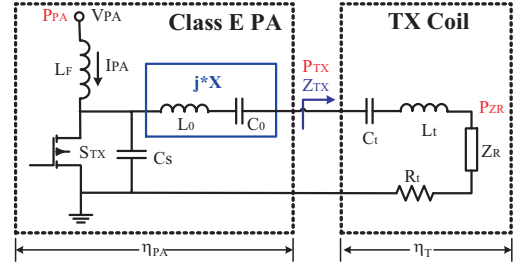


Fig. 2. Circuit topology of the transmitter.

It is well known that the Class E PA can achieve zero-voltage switching (ZVS) operation under a single optimal load, Z_{OPT} . The circuit parameters of the PA can then be optimized targeting this optimal load,

$$\begin{cases} B = \omega C_S = \frac{8}{\pi(\pi^2+4)Z_{OPT}} \approx \frac{0.184}{Z_{OPT}} \\ X = \omega L_0 - \frac{1}{\omega C_0} = \frac{\pi(\pi^2-4)}{16} Z_{OPT} \approx 1.15 Z_{OPT} \end{cases}, \quad (1)$$

where B is the susceptance of C_S , and X is the net reactance of L_0 and C_0 [28]. With Z_{OPT} , PA output power P_{TX} and efficiency η_{PA} can be analytically derived for any PA load, i.e., $Z_{TX} (=R_{TX} + jX_{TX})$,

$$\begin{cases} P_{TX} = \frac{V_{PA}^2 g^2 R_{TX}}{2R_{PA}^2} \\ \eta_{PA} = \frac{g^2 R_{TX}}{2R_{PA}} \end{cases}, \quad (2)$$

where

$$g = \frac{\pi \sin \phi_1 + 2 \cos \phi_1}{2 \cos \phi \sin \phi_1 + \pi/2 \cos \psi}, \quad (3)$$

$$R_{PA} = \frac{\pi^2/4 - g[\pi/2 \cos \phi + \sin \phi]}{\pi B}, \quad (4)$$

$$\psi = \tan^{-1} [(X + X_{TX})/R_{TX}], \quad (5)$$

$$\phi = \tan^{-1} \left[\frac{(\pi^2/2-4) - \pi B R_{TX} \rho (2 \cos \psi + \pi \sin \psi)}{\pi + \pi B R_{TX} \rho (\pi \cos \psi - 2 \sin \psi)} \right], \quad (6)$$

$$\phi_1 = \phi + \psi, \quad (7)$$

$$\rho = \sqrt{1 + [(X + X_{TX})/R_{TX}]^2}. \quad (8)$$

All the above variables, g , R_{PA} , ψ , ϕ , ϕ_1 and ρ , relate to the input impedance of the TX coil, Z_{TX} . As the load of the PA, the TX coil is usually modeled by series-connected L_t , C_t , R_t , and Z_R . Under resonance, the below characteristics of the TX coil can be straightforwardly derived,

$$\begin{cases} Z_{TX} = Z_R + R_t \\ \eta_T = (R_{TX} - R_t)/R_{TX} \\ P_{ZR} = P_{TX}\eta_T \end{cases} \quad (9)$$

The above analytical derivations, (1)–(9), show that the complexity of the transmitter is mainly caused by the load sensitive Class E PA. Theoretically, the behavior of the PA can be analytically predicted for any Z_{TX} when V_{PA} and Z_{OPT} are known. With normalized parameters ($V_{PA}=1$ V and $Z_{OPT} = 1 \Omega$) in (2), Fig. 3(a) and (b) show the influences of R_{TX} and θ_{TX} (i.e., the phase of Z_{TX}) on η_{PA} and P_{TX} . Note that the calculation errors will become large when R_{TX} is small due to the parasitic resistances of the components. It is known that η_{PA} can theoretically achieve 100% when $Z_{TX} = Z_{OPT}$ thanks to the PA's ZVS operation. In practice, high η_{PA} can be ensured within a region of impedance around Z_{OPT} . Since it is inconvenient to analytically represent the impedance region using a constant-efficiency contour, here the high-efficiency region is approximated by a rectangle, as shown in Fig. 3. Specifically the region is defined as

$$\begin{cases} -20^\circ \leq \theta_{TX} \leq 40^\circ \\ 0.6Z_{OPT} \leq R_{TX} \leq 1.2Z_{OPT} \end{cases} \quad (10)$$

Within this region, η_{PA} is high and stable, but P_{TX} can be quite different. Generally, the influence of θ_{TX} on P_{TX} is larger than that of R_{TX} , and P_{TX} increases with a decreasing θ_{TX} for a fixed R_{TX} [see Fig. 3 (b)].

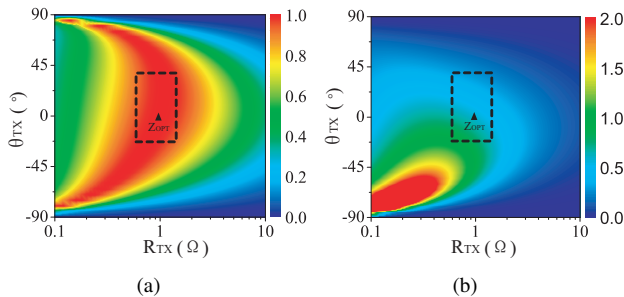


Fig. 3. Characteristics of PA. (a) η_{PA} . (b) P_{TX} .

From a system-level perspective, it is important to ensure a high-efficiency PA in a WPT system. Z_{TX} is expected to be maintained within the high-efficiency region. In this paper, this requirement on Z_{TX} is indirectly fulfilled through tracking the maximum efficiency at the secondary side, i.e., through the MEPT. Thus the high peak efficiency of the Class E PA can always be achieved. Meanwhile, it should be noted that in the high-efficiency region, the PA output power, P_{TX} , significantly varies. This shows that the TX output power capability can actually be modified through tuning Z_{TX} while the high PA efficiency can still be maintained. It indicates that RXs with different power requirements could be charged using the same TX. This possibility is particularly useful to

improve the adaptivity of the multiple-RX WPT system when it is required to charge different devices.

C. Coupling

The load of the transmitter, Z_R , is the reflected impedance of the receivers [refer to Fig. 2 and (9)]. If all the receivers are turned on and charged at the same time, the below relationships exist,

$$Z_R = \sum_{i=1}^n \frac{\omega^2 k_{ti}^2 L_t L_i}{Z_{RX,i}}, \text{ and } P_{ZR} = \sum_{i=1}^n P_{ZRX,i} \quad (11)$$

where k_{ti} is the coupling coefficient between the TX coil and RX_{*i*} coil, $Z_{RX,i}$ is the overall impedance of RX_{*i*}, and $P_{ZRX,i}$ is the power received by RX_{*i*} [2]. Equation (11) shows that the coupling and loading variations of receivers can lead to a complicated Z_R , and in turn make the behavior of the PA unpredictable [refer to (2)–(9)]. The possible cross coupling among RX coils can even lead to a more complicated impedance transformation relationship and adversely affect the power transfer characteristics [4]. Through TDM, i.e., at most one receiver is turned on, (11) is simplified as

$$Z_R = \frac{\omega^2 k_{ti}^2 L_t L_i}{Z_{RX,i}}, \text{ and } P_{ZR} = P_{ZRX,i}, \quad (12)$$

which is straightforward and naturally eliminates the adverse influences of the cross coupling. The inactivated RXs have infinite resistance as loads (i.e., open circuit), namely zero induced current in their RX coils. Thus the inactivated RXs do not disturb the power transfer between the TX and activated RX. Adopting TDM largely simplifies the system modeling and reduces the complexity in design and control.

D. Receiver

Fig. 4 shows a simplified receiver that includes a RX coil and a rectifier. The circuits after the rectifier are represented by a resistive load $R_{DC,i}$, i.e., the input resistance of the buck converter [refer to Fig. 1]. L_i , C_i , and R_i are the inductance, compensated capacitors, and parasitic resistance of the *i*-th RX coil. $Z_{REC,i}$ ($= R_{REC,i} + jX_{REC,i}$) is the rectifier input impedance, namely the load of the RX coil. In the existing design, $Z_{REC,i}$ is usually assumed to be pure resistive. However, this assumption is not valid any more for a WPT system working at Megahertz. The following discussion considers the influence of $X_{REC,i}$ and optimizes the compensation capacitors in order to achieve the desirable power transfer characteristics.

The characteristics of the receiver can be described as

$$\begin{cases} Z_{RX,i} = jX_i + R_i + Z_{REC,i} \\ X_i = \omega L_i - 1/(\omega C_i) \\ \eta_{R,i} = R_{REC,i}/(R_{REC,i} + R_i) \\ P_{REC,i} = \eta_{R,i} P_{ZRX,i} \\ \eta_{REC,i} = P_{DC,i}/P_{REC,i} \end{cases} \quad (13)$$

where X_i is the net reactance of $L_i C_i$, $\eta_{R,i}$ and $\eta_{REC,i}$ are the efficiencies of the RX coil and rectifier, $P_{REC,i}$ and $P_{DC,i}$ are the input power and output power of the rectifier. With conventional secondary compensation, X_i is simply designed

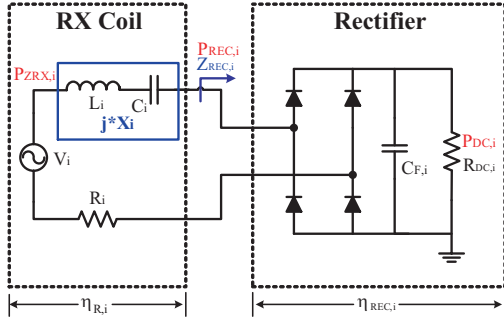


Fig. 4. Circuit topology of the RX coil and rectifier.

to be zero to enhance the RX power receiving capability. However, $Z_{REC,i}$ actually contains obvious reactive components in a MHz WPT system. Thus a proper X_i is expected to compensate the non-zero $X_{REC,i}$ [29]. The influence of X_i can be analytically explained by the impedance relationship between Z_{TX} and X_i . Combining (9), (12), and (13) gives

$$Z_{TX} = R_t + \frac{\omega^2 k_{ti}^2 L_t L_r}{(R_{REC,i} + R_i) + j(X_{REC,i} + X_i)}, \quad (14)$$

which shows X_i affects the performance of PA through Z_{TX} [refer to Fig. 3]. Considering the interactive relationships among the above analyzed circuits, system-level discussion and design are required to properly determine the parameters of the circuits.

III. SYSTEM-LEVEL DESIGN AND CONTROL

A. Design of Transmitter

The output power capability and efficiency of the transmitter are mostly determined by the Class E PA. According to the analysis in section II-B, V_{PA} and Z_{OPT} can serve as two design parameters for the PA [refer to (1)-(9)]. All the other parameters can then be calculated. In a multiple-RX WPT system, the transmitter is expected to be able to efficiently power various kinds of receivers instead of any specific one. A detailed discussion on the PA output power and efficiency is provided as follows.

The output power of PA, P_{TX} , is proportional to V_{PA} [refer to (2)]. Thus increasing V_{PA} can enhance the output capability of the transmitter. However, large V_{PA} should be avoided to lower the voltage stress on S_{TX} ($\approx 3.6V_{PA}$ when $Z_{TX} = Z_{OPT}$) [28]. Considering the breakdown voltage of S_{TX} (150 V) and possible deviation of Z_{TX} from Z_{OPT} , V_{PA} is chosen as 30 V to fully utilize the capability of the switch and ensure a safe margin. Another important parameter is Z_{OPT} that determines the high-efficiency impedance region [refer to Fig. 3]. At the same power level a small Z_{OPT} lowers η_{PA} and η_T because the influences of parasitic resistances of the PA components become obvious. Thus large Z_{OPT} is usually preferred in terms of efficiency. On the other hand, large Z_{OPT} lowers P_{TX} when V_{PA} is given. In this paper, P_{TX} is approximately estimated as 24 W in order to provide 20 W for the final loads. Then a 15Ω Z_{OPT} is calculated by using the specified P_{TX} and V_{PA} in (2). All the circuit parameters of the transmitter are summarized in Table I. L_0 is

a high- Q (310) inductor to ensure the optimal PA operation, and the other parameters of the PA (i.e., X , C_0 , and C_S) can then be calculated by (1). The inductance (L_t) and parasitic resistance (R_t) of the TX coil are measured by a Vector Network Analyzer (VNA). L_t is completely compensated by C_t .

TABLE I
PARAMETERS OF TRANSMITTER

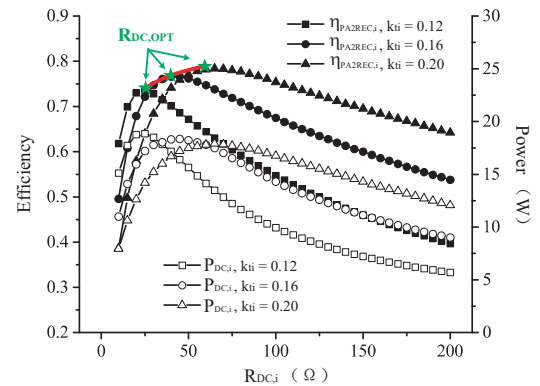
| Frequency | V_{PA} | Z_{OPT} | L_F | S_{TX} | C_S |
|--------------|----------|---------------|--------------|----------|---------------|
| 6.78 MHz | 30 V | 15 Ω | 68 μH | SUD15N15 | 287 pF |
| L_0 | C_0 | X | L_t | C_t | R_t |
| 1.47 μH | 523 pF | 17.3 Ω | 5.40 μH | 104 pF | 1.50 Ω |

B. Design of Receiver

In the receiver, given the RX coil and rectifier, the only unknown parameter that should be properly designed is X_i [see Fig. 4]. According to the above circuit-level analysis, X_i can adjust the power receiving capability of RX_i by compensating the reactive $Z_{REC,i}$ and thus affecting Z_{TX} [refer to (14)]. This is because the PA's characteristics strongly depend on Z_{TX} , i.e., its load [refer to Fig. 3]. The influence of X_i is not straightforward and closely relates to $Z_{REC,i}$ (a function of $R_{DC,i}$). It is challenging to analytically derive the impedance relationship between $Z_{REC,i}$ and $R_{DC,i}$ for a full-bridge rectifier working at MHz. For investigation purposes, system-level simulation is conducted using well-known RF circuit analysis software, the Advanced Design System (ADS) from Keysight Technologies. The parameters in Table I and II are applied in the simulation.

TABLE II
PARAMETERS OF RX COILS AND RECTIFIERS

| L_i | R_i | $C_{F,i}$ | Diode |
|--------------|---------------|------------|----------|
| 1.89 μH | 0.65 Ω | 10 μF | STPSC406 |

Fig. 5. $\eta_{PA2REC,i}$ and $P_{DC,i}$ under different k_{ti} when $X_i = 0$.

Before designing X_i , the system-level characteristics are first discussed under the conventional secondary compensation, i.e., $X_i = 0$. The efficiency from the PA to rectifier is

$$\eta_{PA2REC,i} = \eta_{PA} \cdot \eta_T \cdot \eta_{R,i} \cdot \eta_{REC,i}. \quad (15)$$

Fig. 5 evaluates the influences of $R_{DC,i}$ on $\eta_{PA2REC,i}$ and $P_{DC,i}$ under different k_{ti} . The figure shows that $\eta_{PA2REC,i}$ can be maximized with an optimal load $R_{DC,OPT}$ for each k_{ti} . By tracking these peak efficiencies, namely the optimal loads, such as through the MEPT, the WPT system can always work along the red envelope curve when the coupling varies. The corresponding $P_{DC,i}$ under $R_{DC,OPT}$ is also close to the peak power for a specific k_{ti} . Although Fig. 5 only shows the efficiency-power characteristics from the PA to rectifier, the observation itself can be applicable to the overall system because the buck converter is much less sensitive to the load variation compared to the circuits of the PA, coupling coils, and rectifier [see Fig. 1].

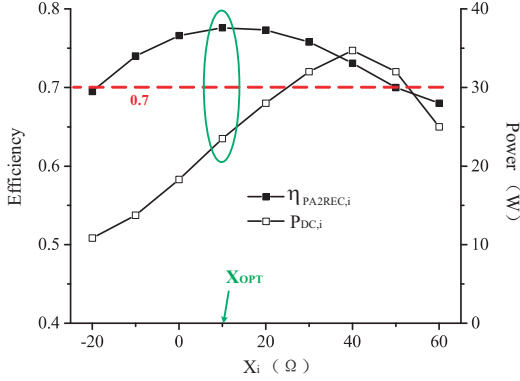


Fig. 6. Maximized $\eta_{PA2REC,i}$ and corresponding $P_{DC,i}$ under different X_i when $k_{ti} = 0.16$ and $R_{DC,i} = R_{DC,OPT}$.

Under different X_i , the maximum efficiency can be tracked in the same manner. These maximized $\eta_{PA2REC,i}$'s and corresponding $P_{DC,i}$'s are summarized in Fig. 6 when $k_{ti} = 0.16$. The purpose of Fig. 6 is to evaluate the influences of X_i under MEPT. The figure shows the maximized $\eta_{PA2REC,i}$ can be improved by having an optimal X_i ($= X_{OPT} = 10 \Omega$). This result can be explained by the relationship between Z_{TX} and X_i , as shown in Fig. 7 [refer to (14)]. The high-efficiency impedance region of the Class E PA defined by (10) is also plotted. When X_{OPT} is applied, Z_{TX} is closest to the target Z_{OPT} ($=15 \Omega$), and thus the maximized $\eta_{PA2REC,i}$ in Fig. 6 is achieved. Note that Z_{TX} can be kept within the defined high-efficiency region of PA when $X_i \in [-20 \Omega, 40 \Omega]$. This shows the high $\eta_{PA2REC,i}$ ($> 70\%$) in Fig. 6 is mostly due to the high-efficiency operation of PA. Under different X_i , even though the maximum efficiency can be tracked, the optimal operation of the overall system does not necessarily guarantee the optimal operation of individual circuits. For instance, the Class E PA may not work exactly at its desired condition, i.e., the ZVS operation. But it still needs to work close to the optimal condition in order to improve the overall system efficiency. Therefore, the maximized $\eta_{PA2REC,i}$ is a compromised solution of the operation of all the circuits.

The influence of X_i on $P_{DC,i}$ in Fig. 6 can also be explained by Fig. 7 and (14). Fig. 7 shows that R_{TX} is relatively stable but θ_{TX} decreases significantly with increasing X_i . This impedance characteristic can lead to increasing P_{TX} and relatively stable η_{PA} when X_i increases [refer to Fig. 3 (a)(b)]. Within the high-efficiency region of PA, the influences of

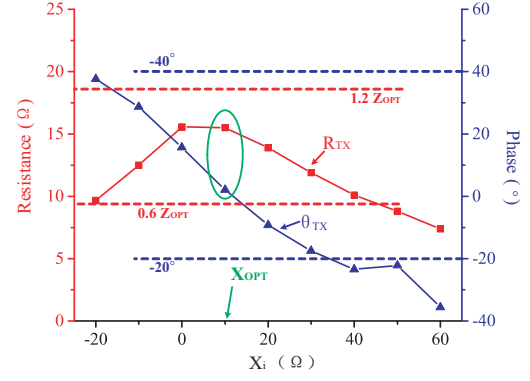


Fig. 7. Z_{TX} under different X_i .

R_{TX} and θ_{TX} on P_{TX} are quite different. It is interesting to find that $P_{DC,i}$ significantly varies when $\eta_{PA2REC,i}$ is high, greater than 70% [refer to Fig. 6]. Such characteristic is particularly useful for a high-efficiency multiple-RX system because different power receiving capability can be achieved by simply using different secondary compensation in a specific receiver. This advantage helps to simplify the design of the receivers and also improves the functionality and adaptivity of the transmitter.

C. Maximum Efficiency Point Tracking

Maximum efficiency point tracking (MEPT) can be applied based on the result showing in Fig. 5. The MEPT is now being widely used in various electrical systems [27]. It was used in one-RX WPT systems, in which the tracked efficiency does not include the efficiency of PA, a standard RF one [30]. A bulky bi-directional coupler is required to measure the input power of the TX coil. This paper extends the MEPT of one-RX system to the proposed TDM-based multiple-RX system, in which the PA efficiency is included. A buck converter is used to achieve the MEPT by controlling $R_{DC,i}$, as shown in Fig. 8. Here $V_{DC,i}$, $V_{OUT,i}$, $I_{DC,i}$, and $I_{OUT,i}$ are the input and output voltages and currents of the buck converter, respectively. For an ideal buck converter,

$$D_i = \frac{V_{OUT,i}}{V_{DC,i}} = \frac{V_{OUT,i}}{\sqrt{R_{DC,i}P_{DC,i}}}, \quad (16)$$

where D_i is the duty cycle of the switch $S_{BUCK,i}$. For each specific relative position of coils, i.e., k_{ti} , there exists an optimal D_i to maximize the overall system efficiency. Meanwhile, the receiver can be turned off by setting D_i as zero. Thus the TDM-based control can also be implemented using the buck converter.

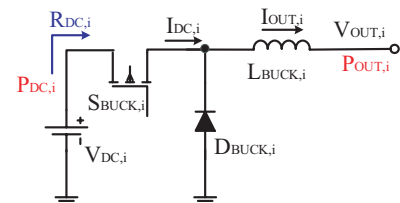


Fig. 8. Buck converter.

The MEPT control block diagram is shown in Fig. 9. At any time, there is at most one receiver being charged. Each receiver has its own RX controller and communicates with the TX controller through WiFi. The controllers obtain the efficiency $\eta_{SYS,i}$ (from the PA to the buck converter) by measuring V_{PA} , I_{PA} , $V_{OUT,i}$ and $I_{OUT,i}$, i.e.,

$$\eta_{SYS,i} = \eta_{PA2REC,i} \cdot \eta_{BUCK,i} = \frac{V_{OUT,i} I_{OUT,i}}{V_{PA} I_{PA}}, \quad (17)$$

where $\eta_{BUCK,i}$ is the efficiency of the buck converter. Note that the tracked efficiency is $\eta_{SYS,i}$ instead of $\eta_{PA2REC,i}$. Because a high $\eta_{BUCK,i}$, usually greater than 90%, can be achieved over a wide range of load [30], it has a limited influence on the value of $R_{DC,OPT}$. In this paper, a simple perturbation and observation (P&O) based method is applied to track the maximum $\eta_{SYS,i}$. The tracking algorithm has been reported in [30].

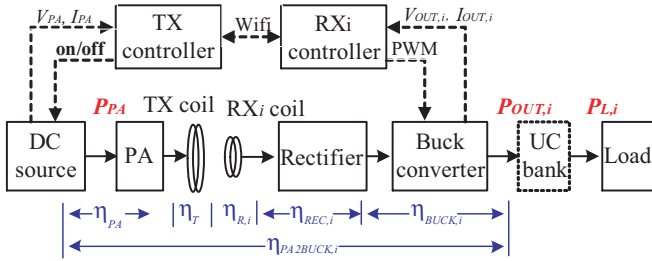


Fig. 9. Control block diagram of MEPT.

D. TDM-Based Power Flow Management

In real applications, there always exist various uncertainties such as in the required power levels, types of power, and coupling conditions. The possibilities of involving those uncertainties can significantly increase when the number of the receivers is varying. As discussed in section II-C, the TDM-based scheme simplifies the analysis of the multiple-RX system, and thus helps to reduce the difficulties in the design and control caused by the complicated coupling conditions among RXs. With TDM, the charging time can be utilized as a new degree of freedom in control. The power flow is straightforwardly managed among the receivers by controlling the charging time of each RX. Thus most of the existing control approaches developed for one-RX systems can be directly applied. This paper explores a new control scheme by applying the MEPT in a TDM-based multiple-RX WPT system, in which the efficiency control and power control are simultaneously achieved. Through introducing load-independent sources or proper control on TX side, it is possible to manage the input power and maintain high efficiency of the TX side. But it is still difficult to guarantee the overall system efficiency without TX-RX communication. Therefore, feedback-based control is attractive for achieving high efficiency in a dynamic environment, where the above uncertainties exist.

Besides, for most power converters, their efficiency usually decreases significantly at light load condition. This issue becomes even worse in a multiple-RX system because its load range is n time wider than that of a one-RX system.

With the control scheme of combining MEPT and TDM, the transmitter does not require any adjustment or control. Both its dc input voltage and operating frequency are fixed. The WPT system can always work at its desired power level with the peak efficiency. Therefore, the transmitter is able to charge receivers under quite different load conditions without sacrificing the power transfer capability. The design of RXs by having different X_i 's also achieves different power receiving ability. In terms of hardware complexity, only the dc input and output are used as feedback signals, which can both be easily measured. The above advantages largely simplify the design and control efforts for multiple-RX WPT systems, and improve the functionality and adaptivity of the systems.

As shown in Fig. 9, a UC bank can be added after the buck converter as an energy buffer in order to continuously power the final load. The UC banks are optional and could be removed if continuous charging is not required. Another advantage of the UC banks is that they can decouple $P_{L,i}$ (the final power requirement) from $P_{OUT,i}$ (the actual output power of the WPT system). Thus both the stability of MEPT and power response time can be improved. This advantage is particularly useful for the systems using load-sensitive resonant converters such as the Class E PA.

A voltage range for the UC bank needs to be first defined (i.e., $V_{OUT,i} \in [V_{OUT,MIN}, V_{OUT,MAX}]$) to ensure sufficient power storage capability and avoid overcharge. The upper and lower limits should be determined based on a specific target application. This paper focuses on the initial discussion on the TDM-based multiple-RX WPT systems. Here a straightforward TDM-based charging strategy is developed involving the below two basic rules.

- Rule 1: If all the $V_{OUT,i}$'s are within the range of $[V_{OUT,MIN}, V_{OUT,MAX}]$, turn off the transmitter.
- Rule 2: If one or more than one $V_{OUT,i}$'s are lower than $V_{OUT,MIN}$, charge the receiver with the lowest $V_{OUT,i}$ until this specific $V_{OUT,i}$ reaches $V_{OUT,MAX}$.

Through the above two rules, the system can automatically turn on and off different RXs according to the UC bank voltages. Note that the TDM-based strategy can be modified for a system without energy buffer. A simple strategy is to assign the charging time t_i for RX_i proportional to its power requirement in a period T , i.e., $t_i : T = P_{L,i} : \sum_{i=1}^n P_{L,i}$. In the proposed system, V_{PA} is designed to make sure that all the RXs can receive sufficient power when the number of RXs reaches its upper limit. When the number of RXs decreases, V_{PA} is kept to be fixed in order to maximize the output power capability of TX, which in turn minimizes the charging time of RXs.

IV. EXPERIMENTAL VERIFICATION

A three-receiver WPT system is built up, as shown in Fig. 10. The system includes one transmitter and three identical receivers. On the TX side, a dc source is used to provide a constant V_{PA} ($=30$ V) to a 6.78 MHz Class E PA; a TX coil is driven by the PA; and a computer is used as the TX controller which directly reads the system input power P_{PA}

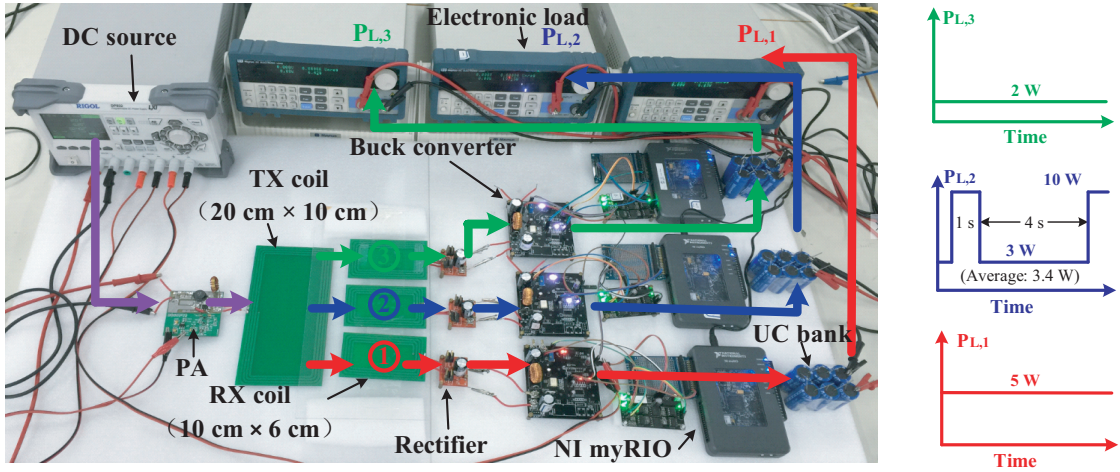


Fig. 10. Experimental setup.

from the dc source. Each receiver consists of a RX coil, a rectifier, a buck converter, a RX controller (NI myRIO), a UC bank and an electronic load. $V_{OUT,i}$ and $I_{OUT,i}$ can be measured and read by the RX controller. All the RX controllers communicate with the TX controller through WiFi. Although the control circuits cause additional power losses, these losses have quite limited influence on the whole system efficiency considering the output power level of the WPT system (> 20 W). The programmable electronic load is also controlled to emulate various power levels and types of the load, $P_{L,i}$. All the RX coils are fixed and placed right above the TX coil. The vertical distance between RX coils and TX coil is 20 mm with coupling coefficients, $k_{t1} = 0.16$, $k_{t2} = 0.15$, and $k_{t3} = 0.15$. The system parameters are given in Table I-III.

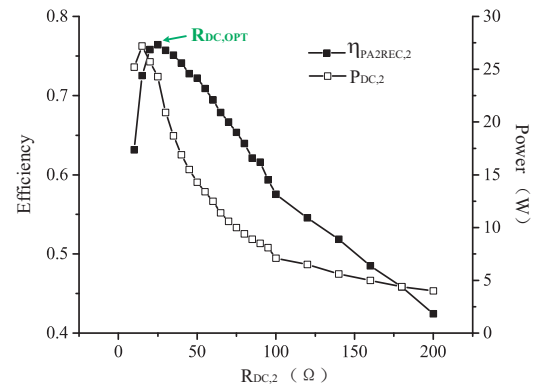
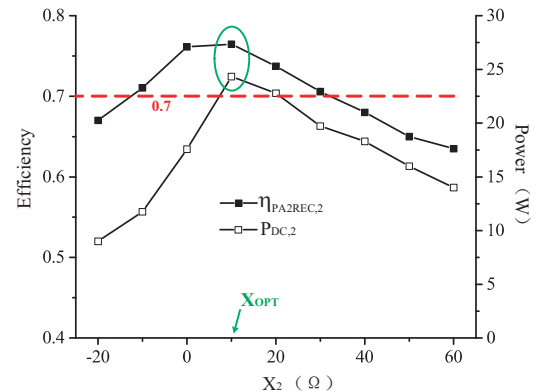
TABLE III
PARAMETERS OF UC BANK

| Cell | Capacitance | $V_{OUT,MIN}, V_{OUT,MAX}$ |
|-----------------------|-------------------------------|----------------------------|
| BCAP0100 (Maxwell) | 16.7 F (6 cells in series) | [10 V, 15 V] (bank) |

A. Influences of $R_{DC,i}$ and X_i

First the electronic load is directly connected to the rectifier without including the buck converter and UC bank. Thus the system-level characteristics in section III-B can be verified under different $R_{DC,i}$ and X_i . Here only RX_2 is activated for verification purpose. Fig. 11 gives $\eta_{PA2REC,2}$ and $P_{DC,2}$ under different $R_{DC,2}$. It validates the existence of the maximum efficiency point, which matches the simulation results in Fig. 5. Fig. 12 shows the influence of X_2 on the maximized $\eta_{PA2REC,2}$ and corresponding $P_{DC,2}$. The basic trend is consistent with that in Fig. 6. An optimal X_2 exists ($X_{OPT}=10 \Omega$) to maximize $\eta_{PA2REC,2}$. The measured $P_{DC,2}$ is slightly different with the simulated result. This is mainly due to the parasitic resistances of the components and measurement errors in the coupling coefficient. It can be seen that the efficiency and power vary with different X_i . This result validates that the power receiving capability of RXs can

be properly designed through the single parameter of RX, X_i . In the following experiments, all RXs are designed targeting the same power level and with $X_i=X_{OPT}(=10\Omega)$.

Fig. 11. Measured $\eta_{PA2REC,2}$ and $P_{DC,2}$ under different $R_{DC,2}$.Fig. 12. Influence of X_2 .

B. Dynamic Characteristics

All the circuits in Fig 10 are included to verify the dynamic response of the TDM-based three-RX system. The receivers have the same parameters but with quite different load power

profiles. As shown in Fig. 10, $P_{L,1}$ and $P_{L,3}$ are fixed at 5 W and 2 W, respectively; $P_{L,2}$ is a pulsed one with two power levels of 3 W and 10 W. The proposed TDM-based control determines which receiver should be charged. MEPT is then implemented in the chosen receiver [refer to section III-C and III-D].

The system is initialized with $V_{OUT,1} = V_{OUT,2} = V_{OUT,3} = V_{OUT,MAX} = 15V$. Fig. 13 and Fig. 14 show the dynamic responses of the voltages of the UC banks ($V_{OUT,i}$'s), output power of the buck converters ($P_{OUT,i}$'s), and input power of the PA (P_{PA}). From t_0 to t_1 , all $V_{OUT,i}$'s stay within the range of $[V_{OUT,MIN}, V_{OUT,MAX}]$, and thus the TX is turned off. Different voltage drop rates are observed due to the difference in $P_{L,i}$'s [see Fig. 10]. At t_1 , $V_{OUT,1}$ first reaches $V_{OUT,MIN}$ (=10 V) and RX_1 is turned on accordingly. The MEPT is implemented until $V_{OUT,1}$ reaches $V_{OUT,MAX}$ (=15 V) at t_2 . Then RX_2 is turned on rightly after RX_1 is turned off because $V_{OUT,2}$ has dropped below 10 V. A similar charging process is repeated after t_3 .

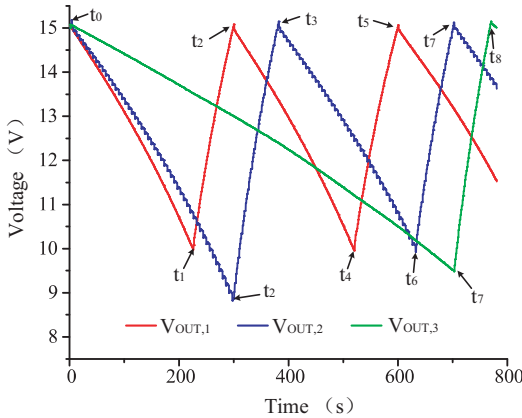


Fig. 13. Voltages of UC banks.

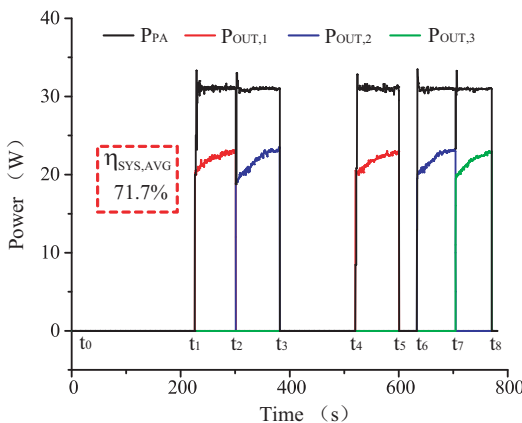


Fig. 14. PA input power and output power of buck converters.

Both Fig. 13 and Fig. 14 show that the receivers can be stably charged under various load power profiles ($P_{L,i}$'s). Because the UC banks decouple $P_{L,i}$ from the WPT system, each receiver can be charged at the maximized $\eta_{SYS,i}$. Even under the pulsed $P_{L,2}$, only small fluctuations in $V_{OUT,2}$ is observed [see the blue curve in Fig. 13]. The stable P_{PA}

and $P_{OUT,2}$ in Fig. 14 indicate that the pulsed $P_{L,2}$ almost has no influence on MEPT. This result also shows that the power response of the system is sufficiently fast even under the pulsed $P_{L,2}$. A stable P_{PA} but slightly increasing $P_{OUT,i}$ are observed in Fig. 14. It is because a higher UC voltage results in a higher efficiency of the buck converter. During the time interval $[t_0, t_8]$, the average system efficiency $\eta_{SYS,AVG}$ is 71.7%. This high efficiency validates the benefit of applying MEPT in a TDM-based multiple-RX WPT system.

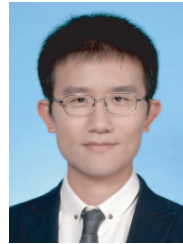
V. CONCLUSION

This paper provides a comprehensive discussion on the characteristics of a MHz multiple-RX WPT system. Through the combination of TDM and MEPT, the power flow management and maximum efficiency can be simultaneously achieved. The Class E PA is introduced to fully utilize its high efficiency and the advantage of MEPT. Based on the circuit models, the system parameters are designed and optimized at a system level. Experimental results show that the example multiple-RX system quickly tracks the maximum efficiency and meets various power requirements (both constant and pulsed ones). With the proposed design and control scheme, the uncertainties in the multiple-RX WPT systems are significantly reduced. This helps to simplify the design and control of the system, and also improve the functionality and adaptivity. Further work could include the charging time optimization of the TDM-based control.

REFERENCES

- [1] N. B. Carvalho, A. Georgiadis, A. Costanzo, H. Rogier, A. Collado, J. A. García, S. Lucyszyn, P. Mezzanotte, J. Kracek, D. Masotti *et al.*, "Wireless power transmission: R&D activities within europe," *IEEE Trans. Microw. Theory Techn.*, vol. 62, no. 4, pp. 1031–1045, Apr. 2014.
- [2] M. Fu, T. Zhang, C. Ma, and X. Zhu, "Efficiency and optimal loads analysis for multiple-receiver wireless power transfer systems," *IEEE Trans. Microw. Theory Techn.*, vol. 63, no. 3, pp. 801–812, Mar. 2015.
- [3] K. Lee and D.-H. Cho, "Analysis of wireless power transfer for adjustable power distribution among multiple receivers," *IEEE Antennas Wireless Propag. Lett.*, vol. 14, pp. 950–953, Jan. 2015.
- [4] M. Fu, T. Zhang, P. C. K. Luk, X. Zhu, and C. Ma, "Compensation of cross coupling in multiple-receiver wireless power transfer systems," *IEEE Trans. Ind. Informat.*, vol. 12, no. 2, pp. 474–482, Apr. 2016.
- [5] M. Q. Nguyen, Y. Chou, D. Plesa, S. Rao, and J.-C. Chiao, "Multiple-inputs and multiple-outputs wireless power combining and delivering systems," *IEEE Trans. Power Electron.*, vol. 30, no. 11, pp. 6254–6263, Nov. 2015.
- [6] K. K. Ean, B. T. Chuan, T. Imura, and Y. Hori, "Impedance matching and power division using impedance inverter for wireless power transfer," *IEEE Trans. Ind. Appl.*, vol. 50, no. 3, pp. 2061–2070, May 2014.
- [7] J. Kim, D.-H. Kim, and Y.-J. Park, "Analysis of capacitive impedance matching networks for simultaneous wireless power transfer to multiple devices," *IEEE Trans. Ind. Electron.*, vol. 62, no. 5, pp. 2807 – 2813, May 2015.
- [8] J. Bito, S. Jeong, and M. M. Tentzeris, "A real-time electrically controlled active matching circuit utilizing genetic algorithms for wireless power transfer to biomedical implants," *IEEE Trans. Microw. Theory Techn.*, vol. 64, no. 2, pp. 365–374, Feb. 2016.
- [9] G. Lee, B. H. Waters, Y. G. Shin, J. R. Smith, and W. S. Park, "A reconfigurable resonant coil for range adaptation wireless power transfer," *IEEE Trans. Microw. Theory Techn.*, vol. 64, no. 2, pp. 624–632, Feb. 2016.
- [10] J. Kim, D.-H. Kim, J. Choi, K.-H. Kim, and Y.-J. Park, "Free-positioning wireless charging system for small electronic devices using a bowl-shaped transmitting coil," *IEEE Trans. Microw. Theory Techn.*, vol. 63, no. 3, pp. 791–800, Mar. 2015.

- [11] P. S. Riehl, A. Satyamoorthy, H. Akram, Y.-C. Yen, J.-C. Yang, B. Juan, C.-M. Lee, F.-C. Lin, V. Muratov, W. Plumb *et al.*, "Wireless power systems for mobile devices supporting inductive and resonant operating modes," *IEEE Trans. Microw. Theory Techn.*, vol. 63, no. 3, pp. 780–790, Mar. 2015.
- [12] Z. Pantic, K. Lee, and S. M. Lukic, "Receivers for multifrequency wireless power transfer: Design for minimum interference," *IEEE Trans. Emerg. Sel. Topics Power Electron.*, vol. 3, no. 1, pp. 234–241, Mar. 2015.
- [13] D. Ahn and P. Mercier, "Wireless power transfer with concurrent 200 kHz and 6.78 MHz operation in a single transmitter device," *IEEE Trans. Ind. Electron.*, vol. 31, no. 7, pp. 5018–5029, Jul. 2016.
- [14] M. J. Chabalko and A. P. Sample, "Three-dimensional charging via multimode resonant cavity enabled wireless power transfer," *IEEE Trans. Power Electron.*, vol. 30, no. 11, pp. 6163–6173, Nov. 2015.
- [15] P. Raval, D. Kacprzak, and A. P. Hu, "Multiphase inductive power transfer box based on a rotating magnetic field," *IEEE Trans. Ind. Electron.*, vol. 62, no. 2, pp. 795–802, Feb. 2015.
- [16] C. Zhang, D. Lin, and S. Hui, "Basic control principles of omnidirectional wireless power transfer," *IEEE Trans. Power Electron.*, vol. 31, no. 7, pp. 5215–5227, Jul. 2016.
- [17] L. Shi, Z. Kabelac, D. Katabi, and D. Perreault, "Wireless power hotspot that charges all of your devices," in *Proc. of the 21st Annu. Int. Conf. Mobile Computing and Networking*, Paris, France, Sep. 2015, pp. 2–13.
- [18] N. Kim, K. Kim, J.-Y. Choi, and C.-W. Kim, "Adaptive frequency with power-level tracking system for efficient magnetic resonance wireless power transfer," *Electron. Lett.*, vol. 48, no. 8, pp. 452–454, Apr. 2012.
- [19] P. C. Loh and D. G. Holmes, "Analysis of multiloop control strategies for l_c/l_f -filtered voltage-source and current-source inverters," *IEEE Trans. Ind. Appl.*, vol. 41, no. 2, pp. 644–654, Apr. 2005.
- [20] S. Aldhafer, P. C.-K. Luk, and J. F. Whidborne, "Electronic tuning of misaligned coils in wireless power transfer systems," *IEEE Trans. Power Electron.*, vol. 29, no. 11, pp. 5975–5982, Nov. 2014.
- [21] L. Scott, "Efficient communication system using time division multiplexing and timing adjustment control," U.S. Patent 5 745 484, April 28, 1998.
- [22] J. Boys, G. Covic, and A. W. Green, "Stability and control of inductively coupled power transfer systems," *IEE Proc. Electr. Power Appl.*, vol. 147, no. 1, pp. 37–43, Jan. 2000.
- [23] B. H. Waters, P. R. Fidelman, J. D. Raines, and J. R. Smith, "Simultaneously tuning and powering multiple wirelessly powered devices," in *Wireless Power Transfer Conf.*, Boulder, CO, USA, May 2015, pp. 1–4.
- [24] Y.-J. Kim, D. Ha, W. Chappell, and P. Irazoqui, "Selective wireless power transfer for smart power distribution in a miniature-sized multiple-receiver system," *IEEE Trans. Ind. Electron.*, vol. 63, no. 3, pp. 1853–1862, Mar. 2016.
- [25] B. Lee, D. Ahn, and M. Ghovanloo, "Three-phase time-multiplexed planar power transmission to distributed implants," *IEEE Trans. Emerg. Sel. Topics Power Electron.*, vol. 4, no. 1, pp. 263–272, Mar. 2016.
- [26] M. Fu, H. Yin, M. Liu, and C. Ma, "Loading and power control for a high-efficiency class E PA-driven megahertz WPT system," *IEEE Trans. Ind. Electron.*, vol. 63, no. 11, pp. 6867–6876, Nov. 2016.
- [27] J. A. Abu-Qahouq, H. Mao, H. J. Al-Atrash, and I. Batarseh, "Maximum efficiency point tracking (MEPT) method and digital dead time control implementation," *IEEE Trans. Power Electron.*, vol. 21, no. 5, pp. 1273–1281, Sep. 2006.
- [28] F. H. Raab, "Idealized operation of the class E tuned power amplifier," *IEEE Trans. Circuits Syst.*, vol. 24, no. 12, pp. 725–735, Dec. 1977.
- [29] M. Fu, Z. Tang, M. Liu, C. Ma, and X. Zhu, "Full-bridge rectifier input reactance compensation in megahertz wireless power transfer systems," in *IEEE PELS Workshop on Emerging Technologies: Wireless Power*, Daejeon, Korea, Jun. 2015, pp. 1–5.
- [30] M. Fu, H. Yin, X. Zhu, and C. Ma, "Analysis and tracking of optimal load in wireless power transfer systems," *IEEE Trans. Power Electron.*, vol. 30, no. 7, pp. 3952–3963, Jul. 2015.



and circuit design optimization.

Minfan Fu (S'13-M'16) received the B.S., M.S., and Ph.D. degrees in electrical and computer engineering from University of Michigan-Shanghai Jiao Tong University Joint Institute, Shanghai Jiao Tong University, Shanghai, China in 2010, 2013, and 2016, respectively.

He is currently a postdoctoral researcher at the Center for Power Electronics Systems, Virginia Polytechnic Institute and State University, Blacksburg, VA, USA. His research interests include megahertz wireless power transfer, resonant converters,



He Yin (S'13) received the B.S. degree in electrical and computer engineering from University of Michigan-Shanghai Jiao Tong University Joint Institute, Shanghai Jiao Tong University, Shanghai, China in 2012, where he is currently working toward the Ph.D. degree.

His research interests include optimization and decentralized control of hybrid energy systems and wireless power transfer systems.



Chengbin Ma (M'05) received the B.S. (Hons.) degree in industrial automation from East China University of Science and Technology, Shanghai, China, in 1997, and the M.S. and Ph.D. degrees in electrical engineering from The University of Tokyo, Tokyo, Japan, in 2001 and 2004, respectively.

He is currently an associate professor of electrical and computer engineering at University of Michigan-Shanghai Jiao Tong University Joint Institute, Shanghai Jiao Tong University, Shanghai, China. Between 2006 and 2008, he held a postdoctoral position with the Department of Mechanical and Aeronautical Engineering, University of California Davis, California, USA. From 2004 to 2006, he was a R&D researcher with Servo Laboratory, Fanuc Limited, Yamanashi, Japan. He is an associate editor of the *IEEE Transactions on Industrial Informatics*. His research interests include networked energy systems, wireless power transfer, and mechatronic control.